Three-dimensional simulation of rocket nozzles with multi-jet interaction using shock-unsteadiness model

Pratikkumar Raje* and Krishnendu Sinha†
Department of Aerospace Engineering, Indian Institute of Technology Bombay, Mumbai 400 076, India

The interaction of supersonic underexpanded exhaust jets for a four-nozzle clustered rocket configuration is studied using three-dimensional RANS simulations. Such interactions can lead to reversed flow of the nozzle exhaust gases towards the base, and result in high pressure and heat loads on the vehicle. Multi-jet interaction flow fields are characterised by a number of shocks and expansion waves, along with turbulent shear layers enclosing subsonic recirculating zones. The complexity of the flowfield is broken down by identifying various viscous/inviscid interactions, with particular focus on the interaction of turbulence with shockwaves. The shock-unsteadiness k-ω turbulence model is used to capture the physics of shock-turbulence interaction, and its effect on the multi-jet flow field.

I. Introduction

The clustering of multiple engines and hence exhaust nozzles for thrust generation is a common practice followed in rocket propulsion. At high altitudes, the underexpanded jets coming out from the neighbouring nozzles expand rapidly. The radial expansion of these jets leads to their mutual interaction which can result in exhaust reverse flow towards the rocket engine base. The jet interaction process and the resulting reverse flow is primarily governed by a parameter called nozzle pressure ratio (NPR), which is defined as the ratio of nozzle exit static pressure to free-stream static pressure. As NPR increases, the exhaust reverse flow changes from subsonic to supersonic regime and its impingement on the rocket engine base creates a stagnation region with high values of heat flux and pressure. This can have significant effect on the rocket performance, in terms of drag/thrust and base heating. It is therefore important to understand multi-jet interaction and predict them accurately.

The works of Goethert [1], Page and Dixon [2], and Lamb et al. [3], Marion et al. [4], and Taylor and Tou [5] are the major analytical contributions in the area of predicting base pressure and convective heating rates for multi-nozzle configurations. These works divide the complex multi-plume induced reverse flowfield into different components which are then analyzed individually. The final solution for the base pressure and base heat flux makes use of results obtained from the different component analyses. However, such methods provide only qualitative estimates as the solution inherently contain all errors and assumptions present in each component analysis. The complexity of the multi-nozzle configurations and the multi-plume induced reverse flow phenomena has restricted attempts to develop a single analytical model for the entire flowfield.

Experimental investigations of multi-jet interaction have been performed by Goethert and Barnes [6], Goethert [1], Musial and Ward [7], Charczenko and Hayes [8], Cubbage [9], Wasko and Cover [10], Brewer and Craven [11], and Desikan et al. [12]. The main objectives of these tests were to provide base pressure and heating trends due to changes in nozzle pressure ratio and Mach number. Geometric parameters, like nozzle diameter, shape and spacing, were also varied. Additionally, nozzle length and its extension from the base of the vehicle were found to affect the base properties.

CFD simulations of the multi-jet interaction flows are presented by Mehta et al. [13, 14], Nallasamy et al. [15], Ebrahimi [16], Wang [17], Gusman et al. [18], and Deere et al.[19]. Majority of these works aim at providing the best CFD practices for multi-plume simulations by studying the effects of mesh resolution, nozzle exit and other boundary conditions, and multi-species gas model on the base pressure and base heat flux.

The complexity of the multi-jet interaction flows arises due to various flow structures, flow regimes, and large thermal and momentum gradients within the base region. Such flows span from subsonic to supersonic Mach numbers and consists of a multitude of shocks and expansion waves. There are regions of strong inviscid/viscous interactions involving free shear layers, boundary layers, shocks, separated flow and recirculation regions, and plume/plume interaction. Additionally, the flowfield induced by multiple parallel under-expanded jets can be highly three-dimensional. The complex multi-nozzle configuration and the rocket base requires elaborate grid generation and thus CFD simulation of

*Graduate student, Department of Aerospace Engineering, Indian Institute of Technology Bombay.
†Professor, Department of Aerospace Engineering, Indian Institute of Technology Bombay, and AIAA Senior Member.

these flows is an exceptionally challenging task. However, three-dimensional Renolds-averaged Navier-Stokes (RANS) simulations still remain a viable option to predict the multi-jet interaction flowfield and the associated base pressure and base heat flux.

The strength of reverse flow due to multi-jet interaction mainly depends on the level of turbulence in the interacting plume shear layers. Therefore, prediction of base pressure and base heat flux is sensitive to the choice of turbulence model. The multi-jet interaction flowfield has shock waves interacting with the turbulent plume shear layers and turbulence gets amplified across these shock waves. Conventional turbulence models like the standard k-ϵ, k-ω, and Spalart-Allmaras grossly overpredict turbulence amplification across shock waves [20, 21]. The turbulence intensity or the level of eddy viscosity μ_T in the plume shear layers influences the plume expansion [18, 19] thereby affecting the multi-jet interaction flowfield and the reverse flow.

The shock-unsteadiness (SU) k-ω model of Sinha et al. [20] is found to be a better choice over the conventional turbulence models for flows involving shock waves interacting with turbulent boundary layers [21–24] and turbulent free shear layers [25]. The SU model is based on linear inviscid analysis of shock-turbulence interaction and incorporates the underlying physics. It predicts a lower amplification of turbulence kinetic energy across a shock wave compared to the conventional models and matches the DNS data well for a range of Mach numbers. The shock-unsteadiness correction is applied only at shock waves, and the original k-ω model is recovered elsewhere in the computational domain. In this work, we apply the SU k-ω model to the problem of multi-jet interaction.

We study the flowfield of the multi-jet interaction for a four-nozzle rocket system configuration using Reynolds-averaged Navier Stokes (RANS) computation. A three-dimensional multi-block structured grid is used to compute the complex flow field and the flow features are studied in detail. These include expansion fans generated at the nozzle lip, boundary layer separation at the base shoulder, formation of shock waves inside the jets, as well as in the external flow. A number of viscous and inviscid interactions are identified and their effect on the multi-jet interaction is discussed. Finally, regions of turbulent shear layers interacting with shock waves are identified, and the effect of shock-turbulence physics on the flow field prediction is presented.

II. Multi-jet interaction flowfield

Musial and Ward [7] and Mehta et al. [14] put forward a flow model for the base flowfield induced due to multi-jet interaction with the help of wind tunnel experiments and CFD simulations. The flow model is proposed using a four-engine configuration with a flat base and it describes the various base flow regimes due to multi-jet interaction for the ascent of rocket from lift-off to in-space environments. These regimes are observed for all flight NASA launch vehicles [14]. Figure 1 shows one such flow regime for the medium altitude case with moderately underexpanded plumes. The base flowfield observed for the test cases considered in this work falls in this regime and plume induced flow separation is not observed.

Figure 1 shows a schematic of two under-expanded jets interacting along the vehicle center line. We present the main flow features that are expected in the resulting multi-jet interaction. Here, expansion fans are denoted by green lines, shocks by red color, and free-shear layers and boundary layers are shown in grey shade. The details of the flow topology is discussed below, so as to gain insight into the gas dynamic, viscous and turbulence-related phenomena occurring in a multi-jet interaction flowfield.

The boundary layer developed over the vehicle body undergoes an expansion at the base shoulder and separates as a free-shear layer. The free-shear layer encloses the low pressure base flow region with embedded subsonic vortices. At the nozzle exit, the high pressure exhaust gas expands rapidly by generating an expansion fan at the nozzle lip. The jet shear layer separates the exhaust gas from the surrounding flow. The free-shear layers emanating from the base shoulder and the nozzle lip come together near the nozzle-exit plane. This interaction between two supersonic streams forms an external shock and it spreads around the vehicle's rear. Also, an internal shock is formed which is embedded inside the jet plume. This is similar to the barrel shock formed in under-expanded jets exhausted into still air.

The radially expanding plumes from the neighbouring nozzles interact with each other at the model centerline downstream of the nozzle-exit plane. As a result of this mutual impingement, the supersonic exhaust gases are deflected axially, producing a set of trailing shocks inside the interacting plumes. The low-energy gas within the mixing region of the interacting jets is unable to negotiate the adverse pressure of the trailing shock wave and flows back into the base. An inflection point is formed at the intersection of the plumes and the resulting reverse flow is called the "updraft plume". The recirculated mass flows into the center area in a flow passage formed by the jet plume boundaries and the nozzle external walls. It flows radially out of the base through the vent area between the nozzles.

The basic flow topology of a multi-jet interaction is governed by the gas dynamics of shock waves, expansion fans

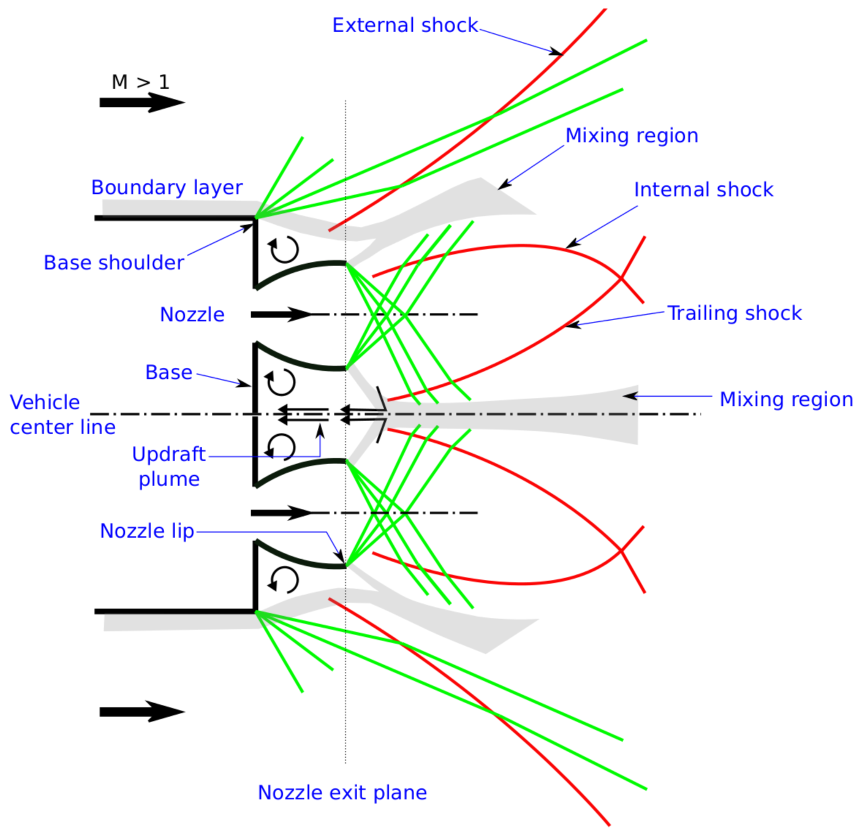

Fig. 1 A schematic showing the multi-jet interaction flowfield and the associated base flow for moderately underexpanded plumes.

and their interactions. The viscous and turbulence effects, on the other hand, decide the thickness of shear layers, and the strength of the reversed flow. A combination of viscous and inviscid phenomena finally determine the base pressure and heat transfer rates. Of particular interest is the interaction of shock waves with turbulence in the flow. Shock-turbulence interaction occurs when shear layers and shock waves come together. The turbulent fluctuations are amplified by a shock wave, and the level of amplification can influence the location of inflection point and the size of the recirculation region enclosed by the shear layer.

Another prominent region for shock-turbulence interaction is the inflection point, where the shear layers from adjacent under-expanded jets come together. Here again, turbulence amplification at the trailing shock can influence the level of turbulence in the reversed flow. Viscous and turbulent dissipation in the updraft flow directly determines the pressure and temperature of the gas at the base stagnation point. The shock-unsteadiness k-ω model is tailor-made based on shock-turbulence physics and validated against DNS data. It is found to give accurate amplification of turbulence kinetic energy at shock waves. It will be interesting to see the effect of SU k-ω model on the multi-jet interaction flowfield, especially in the regions of shock-shear layer interaction.

III. Test case

Musial and Ward [7] conducted experiments on a wind tunnel strut mounted model for several four-nozzle clustered configurations, using bell shaped and conical nozzles. Three different nozzle extension ratios (nozzle extension length from the base to diameter, L/D_e) and different nozzle spacing ratios (nozzle spacing to nozzle exit diameter, D_s/D_e) were considered for a range of NPR and freestream Mach number in the experiments. The present investigation focusses on the experimental configuration that used bell nozzles with D_s/D_e of 2.18 and L/D_e of about 0.7. Three-dimensional simulations are carried out for the underexpanded jets with a NPR of 7.2, where NPR is defined as the ratio of nozzle exit and ambient static pressure. This corresponds to a chamber pressure to ambient static pressure ratio of 990. The freestream Mach number is 2.5. The geometric details and flow conditions are given in Table 2.

Table 1. Viscous/inviscid interactions observed in multi-jet flow field, along with their salient features

Interaction	Representation	Salient features	Multijet flowfield
Inviscid – inviscid interaction			
Oblique shock-expansion fan interaction	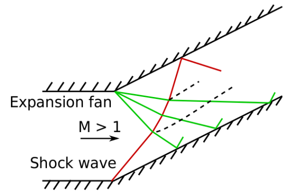	Shock and expansion fan transmit through each other, with reduced strength and altered angle. A set of slip lines emanate from the interaction region.	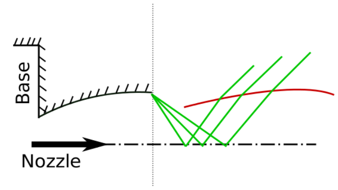
Expansion fan-expansion fan interaction	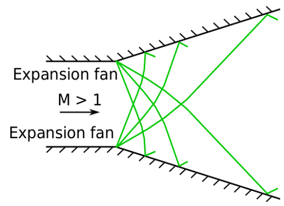	The two identical expansion fans cross each other, with altered deflection angle and strength. Interaction similar to reflection from symmetry line.	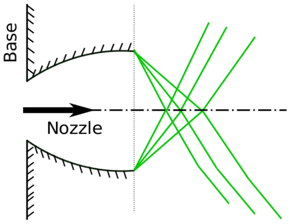
Edney type I oblique shock interaction	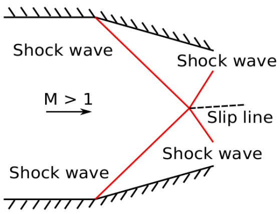	Two shocks of opposite family interact to generate two additional shock waves and a slip line emanates from the triple point.	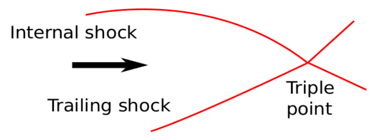
Viscous-invscid interaction			
Free-shear layer expansion fan interaction	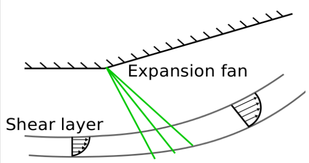	The free shear layer deflects through the expansion fan, which in turn is reflected back as compression waves.	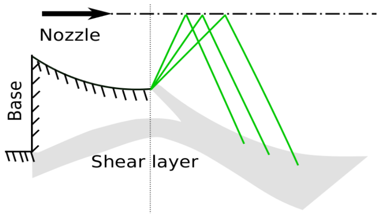
Viscous-viscous interaction			
Free shear layer interacting with a symmetry plane	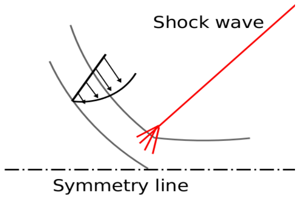	Shear layer deflected along the symmetry plane and an oblique shock wave is formed, which compresses the shear layer.	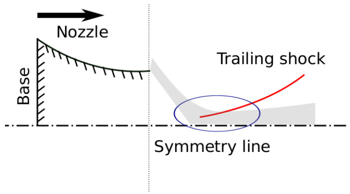
Interaction of two supersonic free shear layers	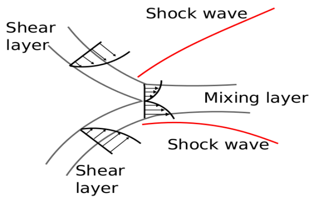	Two oblique shocks are formed on either side of the inflection point and a combined free shear layer is formed downstream. The shocks compress the shear layers and generate reversed flow.	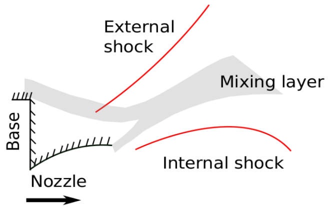

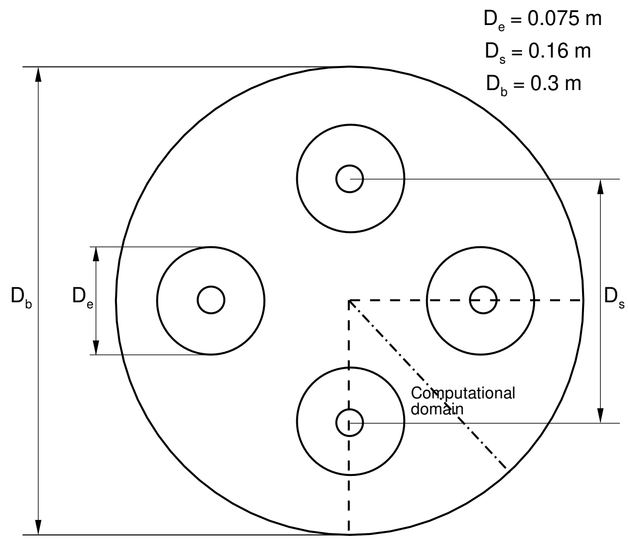

Fig. 2 Base plate with four nozzles and the dash-dotted line shows the region where base pressure and heat flux were measured. Computational domain used for the simulations is shown by dashed lines.

Table 2 Geometry and flow parameters.

Geometry parameter	**Value**
Base diameter, D_b	0.305 m
Nozzle exit diameter, D_e	0.075 m
Nozzle spacing ratio, D_s/D_e	2.18
Nozzle extension ratio, L/D_e	0.7
Nozzle area ratio	12
Flow conditions	**Value**
Base wall temperature, T_d	338.9 K
Chamber pressure, P_c	4.14 MPa
Chamber temperature, T_c	3227.8 K

IV. Simulation Methodology

The multi-jet interaction flow-field is simulated by solving the three-dimensional Reynolds-averaged Navier-Stokes equations with Favre decomposition of the flow variables, as presented in Wilcox [26]. Wilcox 1988 k-ω model is used as the baseline model for turbulence closure. The shock-unsteadiness modification of Sinha et al. [20] is applied over this baseline model. We use a well-validated in-house CFD code that has been employed to a variety of high-speed flow simulations in the past [21–23, 27–30].

The governing equations are discretized in a finite volume formulation where the convective fluxes are computed using a modified, low-dissipation form of the Steger-Warming flux splitting approach [31]. Central differencing is used for the viscous fluxes and turbulent source terms. The turbulence models are fully coupled with the mean flow equations and the CFD solver has been implemented in parallel using the Message Passing Interface (MPI). An implicit full matrix Data-Parallel Lower-Upper Relaxation method [32] is used to integrate the equations in time until steady state is reached.

Perfect gas (thermally and calorically perfect) assumption is used in this work, as previous studies [14, 15] show that reasonable predictions for base pressure and base heat flux can be obtained using these assumptions. The freestream is treated as a perfect gas with $\gamma = 1.4$. The nozzle internal flow is not solved and one-dimensional isentropic flow relations are used to obtain nozzle exit conditions using the chamber pressure and temperature. A value of $\gamma = 1.3$

is considered for the isentropic flow within the nozzle for the combustion gases. In the entire flowfield, perfect gas with $\gamma = 1.4$ is considered. Also, radiation heat transfer is neglected since it is found to be negligible compared to the convective heat transfer for this case [14].

A. Shock-unsteadiness (SU) model

Sinha et al. [20] present a detailed study of shock-turbulence interaction and identify the major physical mechanisms that determine the turbulence amplification at a shock wave. A new shock-unsteadiness effect is identified and is modeled on the basis of linear inviscid theory for shock-turbulence interaction. The modeled transport equation for turbulence kinetic energy (k) takes the following form at shock waves,

$$\frac{\partial \overline{\rho} k}{\partial t} + \frac{\partial \overline{\rho} \widetilde{u_i} k}{\partial x_i} = -\frac{2}{3} \overline{\rho} k \frac{\partial \widetilde{u_i}}{\partial x_i} + \frac{2}{3} b_1' \overline{\rho} k \frac{\partial \widetilde{u_i}}{\partial x_i} - \beta^* \overline{\rho} k \omega \tag{1}$$

where $\beta^* = 0.09$ and the overbar and tilde represent Reynolds and Favre-averaged quantities, respectively, and repetitive indices indicate Einstein summation. The turbulence specific dissipation rate is given by ω, whereas ρ is the density, p is the pressure and u_i is the component of velocity in the x_i direction. The model parameter $b_1' = 0.4(1 - e^{1-M_{1n}})$, where M_{1n} is the shock-normal Mach number in the upstream flow.

The terms on the left-hand side represent the unsteady and convective transport of turbulence kinetic energy (TKE). The first term on the right-hand side represents the production of TKE due to mean dilatation. This replaces the conventional production term in standard turbulence models, and it amplifies turbulence at shock waves. The form of the production term is based on the fact that the mean dilatation is the dominant part of the mean strain rate tensor in the regions of shock waves. Also, the eddy viscosity is set to zero in shocks and high compression regions, because of the breakdown of the underlying Boussinesq approximation [20]. The second term in the above equation represents the shock-unsteadiness modification. It has a form that is very similar to the production by mean dilatation but is opposite in sign. It represents the damping effect of unsteady shock oscillations on the amplification of TKE across a shock wave. The last term represents the viscous dissipation of TKE.

The shock-unsteadiness model given in Eq. (1) is integrated into the Wilcox 1988 k-ω framework by using a shock-identifying function and the strategy used is similar to that presented in Sinha et al. [21]. The implementation is such that the SU correction is applied in the regions of shock waves and the original model is recovered otherwise. To simplify the CFD implementation of the SU model in a complex three-dimensional flowfield, the actual variation of b_1' is not considered. Instead, a constant value of $b_1' = 0.28$ is used in the entire multi-jet interaction flow.

B. 3D multi-block structured grid

Figure 3(a) shows the cross-section of the computational grid, with two nozzles and the corresponding symmetry planes. From symmetry considerations, only $1/8^{th}$ sector of the base can be used for the CFD simulations. However, due to convergence difficulties with such a grid, we use a quarter grid for the simulations (see Fig. 3). A three-dimensional structured multi-block body fitted grid is generated using the commercial software Gridgen. The maximum extension of the domain in the transverse direction is about $3.4D_e$, whereas it extends to about $10D_e$ in the streamwise direction downstream of the base plane and about $8.2D_e$ upstream of the base plane. We use a 7-block structured grid for the computations and the grid consists of a total of 6.27 million interior cells.

Musial and Ward [7] provided co-ordinates of the bell nozzle contour and they are used to generate a two-dimensional curve. This curve is then exported in the Gridgen software and a 3D bell-shaped nozzle contoured grid is generated as shown in Fig. 4. Grid refinement is carried out in the critical regions such as near the wall of upstream extended base, base shoulder, base wall region, nozzle exit, and the plume interaction location. However, neither grid convergence nor grid adaptation is considered due to time and resource constraints.

Figure 5 shows the three-dimensional computational domain along with the boundary conditions used in the simulations. On the base surface, no slip condition for the velocity and constant wall temperature boundary condition are specified. At the inflow boundary upstream of the base, uniform inflow conditions are prescribed. The flow properties at the top and exit boundaries are extrapolated from those of the interior domain. Symmetry boundary conditions are prescribed on the nozzle symmetry plane and uniform flow conditions obtained using one-dimensional isentropic flow relations are specified at the nozzle exit.

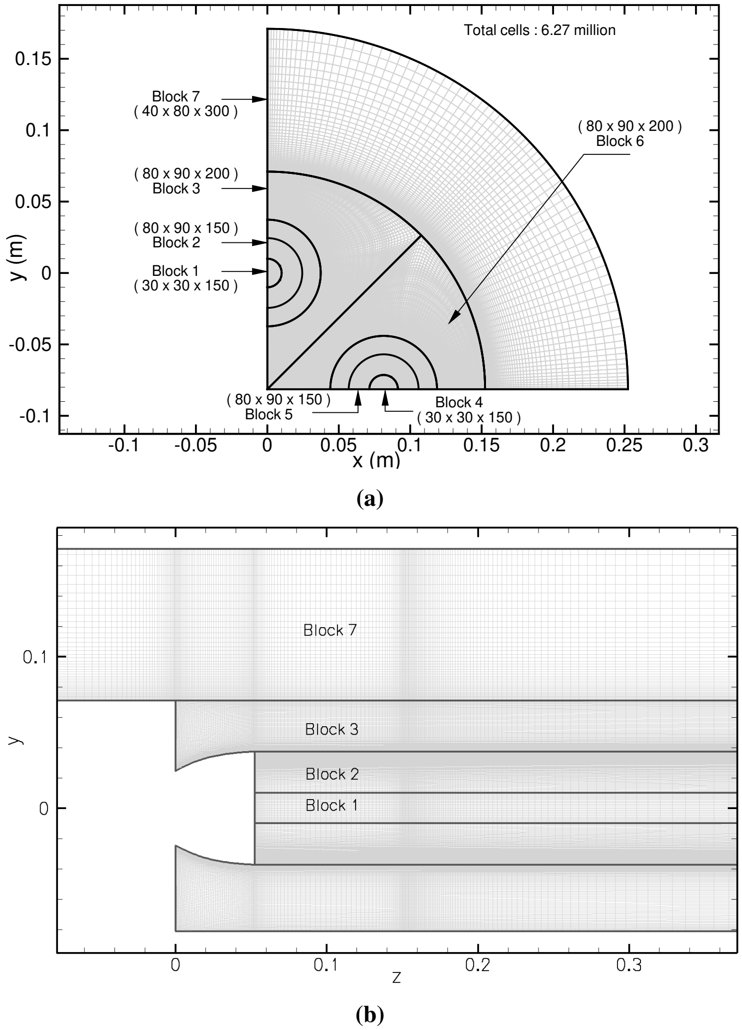

Fig. 3 Three-dimensional multiblock grid used in the simulations (a) cross-sectional view and (b) nozzle symmetry plane.

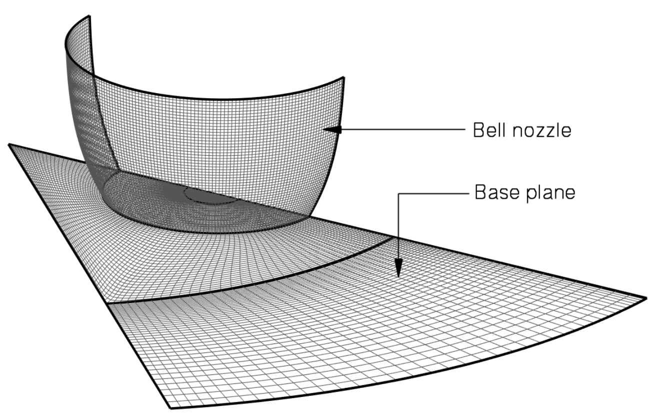

Fig. 4 Grid showing bell shaped nozzle and the base plane used for the simulations.

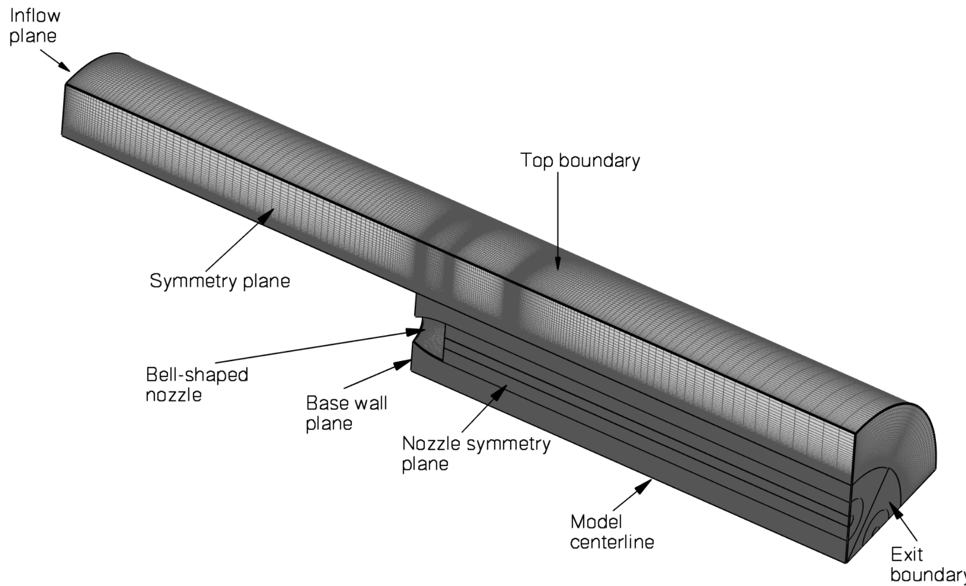

Fig. 5 3D view of the multi-block grid used for the computations along with the boundary conditions employed.

V. Results and Discussion

Figure 6 shows the multi-jet interaction flowfield using the density gradient magnitude contours in the yz symmetry plane. The flowfield and shock structure as obtained using the CFD simulations (Fig. 6) are similar to that described in the schematic shown in Fig. 1. The important flow-features such as the shear layer and expansion fan emanating from the base corner, interaction of the jets and the inflection point, trailing edge shocks formed due to the jet interaction, and jet boundaries are successfully captured in the simulations. The different viscous and inviscid interactions, as seen in Fig. 6 and described in Table 1, give rise to the complexity of the multi-jet interaction flowfield.

Figure 7 shows the three-dimensional view of the flowfield using Mach contours in the two perpendicular symmetry (xy and yz) planes along with the base wall plane. The flow in the two symmetry planes is identical. The Mach 3.7 nozzle exit flow expands to about Mach 7.4 and the pressure decreases by about a factor of 74.5 inside the jet boundaries between the internal and trailing shock waves. The flow then gets compressed by the internal and trailing shocks and an Edney type I interaction between these shock waves is observed. The flow continually expands beyond this interaction. A number of streamlines are drawn in the two symmetry planes to show the flow pattern of the free-stream and the internal jet flow.

The supersonic freestream Mach 2.5 flow over the cylindrical body expands to about Mach 3.6 around the base

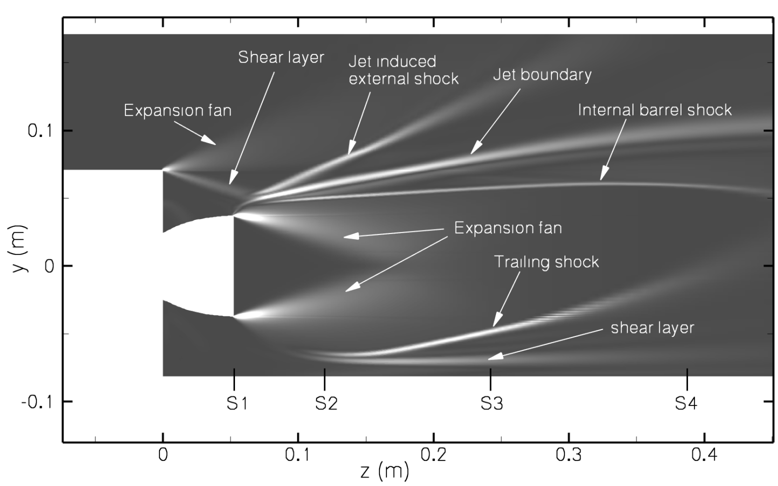

Fig. 6 Density gradient magnitude showing the different flow-features captured by the simulations.

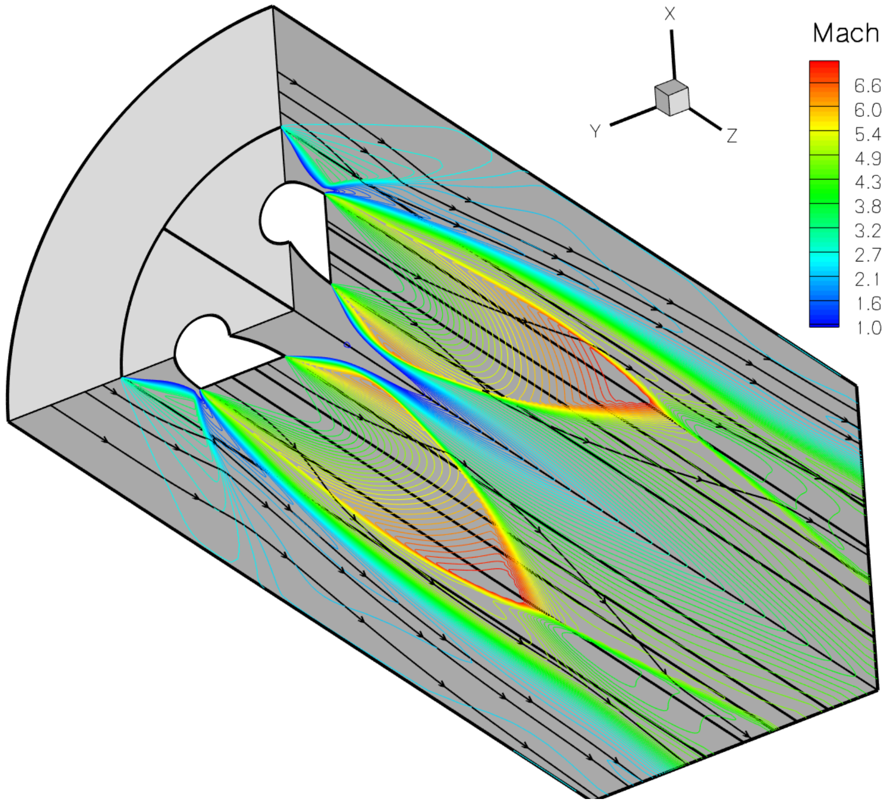

Fig. 7 3D view showing the multi-jet interaction flowfield using the Mach contours.

shoulder and separates as a free-shear layer (see Fig. 8). The free-stream pressure reduces by a factor of about 7 after this expansion and the separated free-shear layer interacts with the jet boundary almost near the nozzle exit plane. The separated free-shear layer and the nozzle wall encloses a subsonic region. The pressure across the free-shear layer and in the enclosed subsonic region is nearly constant and is similar to the pressure after the expansion around the base shoulder.

The interaction between separated free-shear layer and the jet boundary results in the formation of a jet induced external shock outside the jets and a barrel-shaped shock inside the jets. The pressure values after the external shock are higher than the ambient pressure and hence the effective NPR as experienced by the jets is smaller than the NPR of 7.2. The external shock wave interacts with the expansion fan emanated from the base shoulder and increases the pressure by a factor of 5 and more. The strength of this shock wave reduces as we go away from the nozzle exit. The interactions between the freestream flow and the jet boundary causes the jet to experience variable ambient pressure conditions. This results in a pressure distribution that varies along the jet boundaries.

Figure 9 shows the expansion of the lower part of the jet flow in terms of the Mach number and pressure contours in the yz symmetry plane. This lower part of jet flow undergoes greater expansion, from Mach 3.7 to about Mach 6.3, as compared to the top part interacting with the freestream. At the end of the expansion, pressure decreases by a factor of about 20, which is twice compared to the expansion in the top part. The pressure in the subsonic region enclosed by the lower jet-boundary and the nozzle wall is found to be about 1.5 times higher than that observed in the subsonic region enclosed by the free-shear layer emanated from the base corner and the nozzle wall. This higher pressure may be attributed to the jet impingement effect.

Figure 10 shows Mach number and pressure contours in the xy cross-sections at different axial locations; refer Fig. 6 for their exact locations. The evolution of the four jets just after nozzle exit plane till some distance away from the inflection point is presented. Figures 10(a) and 10 (b) show the flow structure in a plane just after the nozzle exit. The jets are fairly circular and they assume the nozzle exit geometry shape. Expansion fan generated at the base shoulder can be seen surrounding the external shock, free-shear layer from the base corner, and the four jets. Subsonic flow is seen in between the nozzles with fairly uniform pressure distribution. Supersonic pockets are seen in the symmetry planes in between the two adjacent jets. The external shock and the free-shear layer are seen to be distorted at the symmetry plane corners and this is a grid artifact as these locations correspond to triple points in the multi-block grid system.

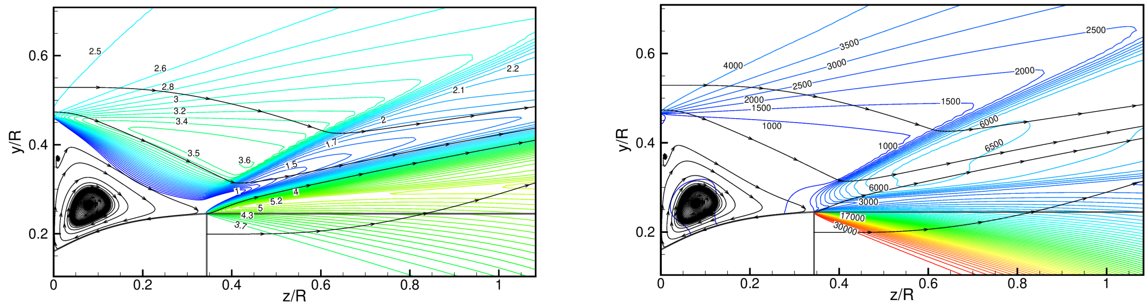

(a) **(b)**

Fig. 8 (a) Mach number and (b) Pressure (Pa) contours showing the expansion at the base shoulder in the yz symmetry plane.

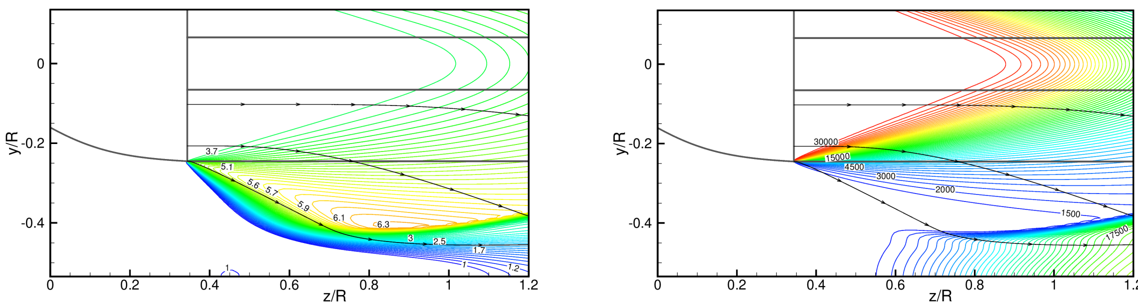

(a) **(b)**

Fig. 9 (a) Mach number and (b) Pressure (Pa) contours showing the lower jet-boundary expansion in the yz symmetry plane.

The radial expansion of the jets results in their mutual interaction downstream of the nozzle exit plane and the interaction location is called as the inflection point. For a symmetric geometry and flow configuration, such as the one considered in this work, the interaction occurs in the symmetry planes (see Figs. 10 (c) and 10 (d)). The jet shear layers get flattened due to the interaction while the outer boundaries remain circular. A saddle point is observed in the interaction plane with part of the jet flow turned towards the center of the four nozzles. Another part of the jet flow moves radially outward towards the jet boundary and results in the protrusion in the external shock wave in the jet interaction plane.

Jet boundary distortion from circular to a pear shape increases downstream, as seen in Figs. 10 (e) and 10 (f). The flow in the jet interaction plane that turns radially inwards toward the model centerline results in a pressure increase and the maximum pressure is observed along the model centerline as seen in Figs. 10 (f) and 10 (h). A high pressure region along the symmetry planes between the two adjacent jets is also observed. By comparison, a low pressure and high Mach number region is observed in the core of each jet. It is influenced by the trailing shock and the internal barrel-shaped shock. The shear layer enclosing all four jets take a square cross-section farther away, as seen in Figs. 10 (g) and 10 (h). Prominent shear layers also develop along the symmetry planes between the adjacent jets.

Figure 11 shows the TKE and μ_T distribution in the region where the trailing shock interacts with the jet boundary. The dilatation contours, shown using black color, identifies the high compression regions of shock waves, and they represent the regions in the flowfield where the SU modification is applied. The external and internal shock waves as well as the trailing edge shock wave interacting with the turbulent shear layers amplify the turbulence levels in these shear layers. The SU correction reduces the TKE amplification and hence the maximum levels of μ_T in the shock-turbulent shear layer interaction regions as compared to the Wilcox 1988 k-ω model. This is evident in the Fig. 11. The SU model significantly reduces the TKE and μ_T levels in the shear layers passing through the trailing shock in comparison with the Wilcox 1988 k-ω model. However, turbulence levels in the reverse flow are nearly identical between the two models. Thus, the overall effect of SU modification is to bring down turbulence levels beyond the shock-shear layer interaction

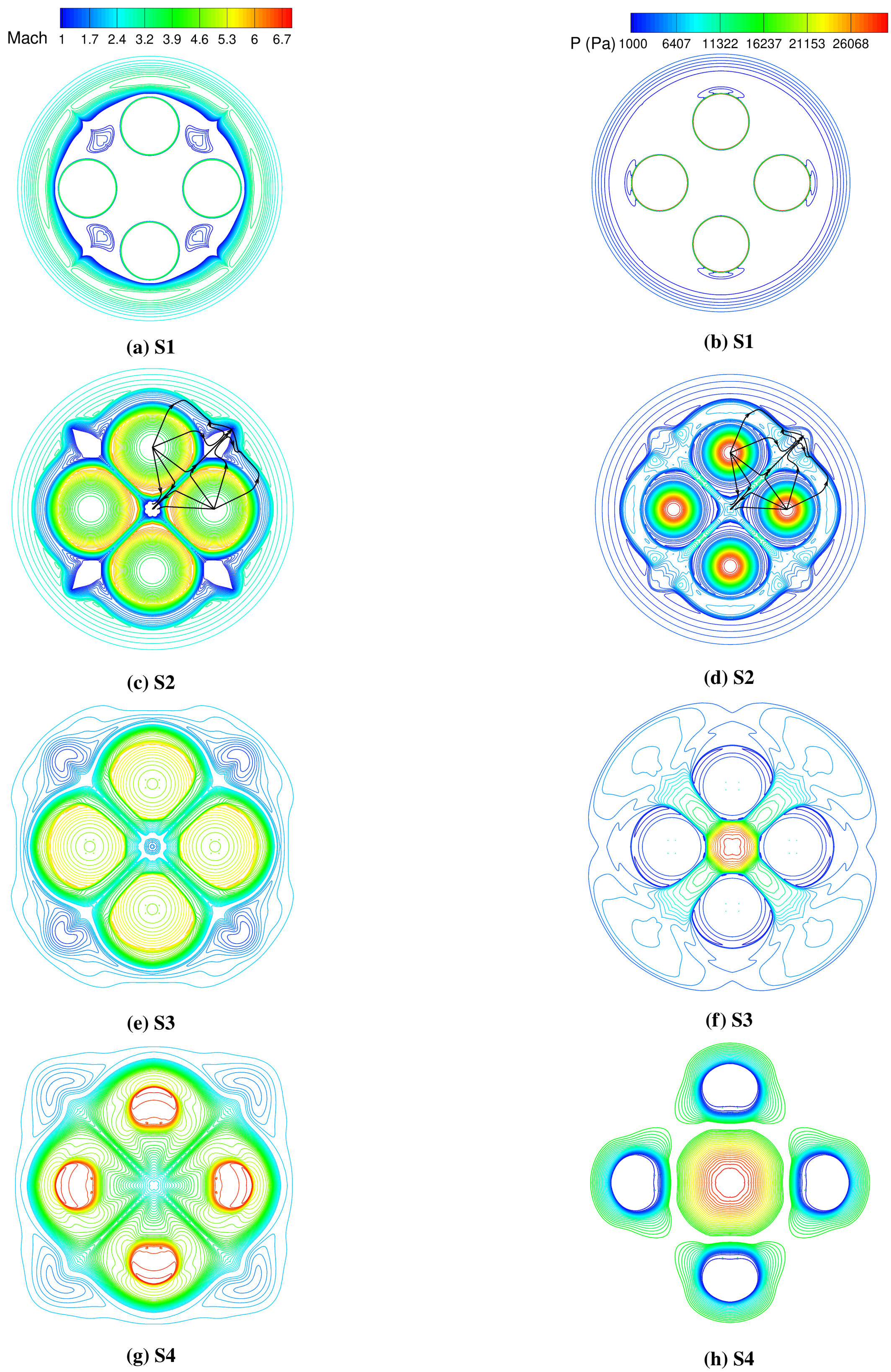

Fig. 10 (a), (c), (e), and (g) Mach number contours and (b), (d), (f), and (h) pressure contours at different xy cross-sections along different axial locations (Refer Fig. 6 for their exact locations).

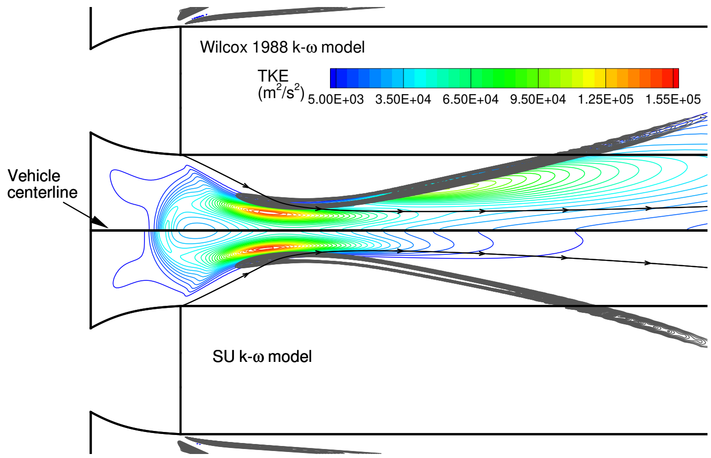

(a)

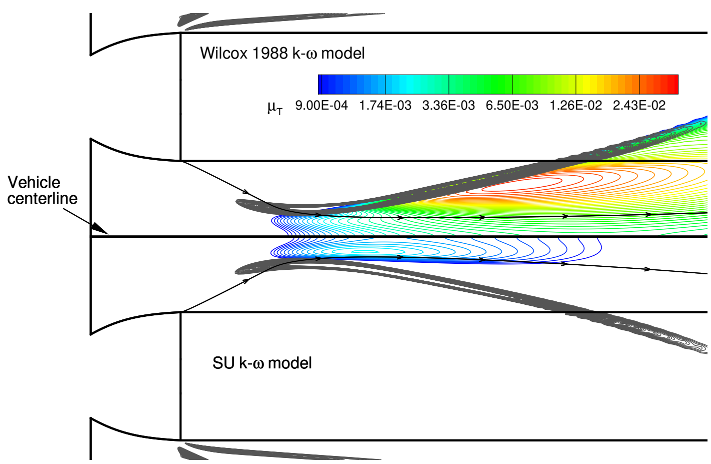

(b)

Fig. 11 Comparison of the distribution of (a) TKE and (b) μ_T as obtained using the Wilcox 1988 k-ω and SU k-ω model. Shocks are idenfied using the negative dilatation contours shown in black color.

regions. On the other hand, the turbulence levels near the base are nearly identical as predicted by the two models.

A streamline, as shown in Fig. 11, is chosen which passes through the trailing shock, to see the effect of SU modification on the TKE and μ_T amplification. Figure 12 shows that SU model predicts a significantly lower TKE and μ_T amplification across the trailing shock and hence the jet boundary passing through the shock also shows lower turbulence levels than that predicted by the Wilcox 1988 k-ω model.

The effect of SU modification is also seen in the inflection point location. Figure 13 shows the sonic line plot for the three cases of laminar, Wilcox 1988 k-ω, and SU model computations. The sonic lines represent the extent of expansion of the turbulent free shear layers or the jet boundaries and identify the inflection point position. Laminar computation predicts jet-jet interaction downstream of the Wilcox 1988 and SU k-ω model computations. The SU modification delays the interaction compared to the Wilcox 1988 model. Laminar and SU model results show a supersonic pocket in the subsonic region between the two interacting jets, which is not predicted in case of the Wilcox 1988 k-ω model computations.

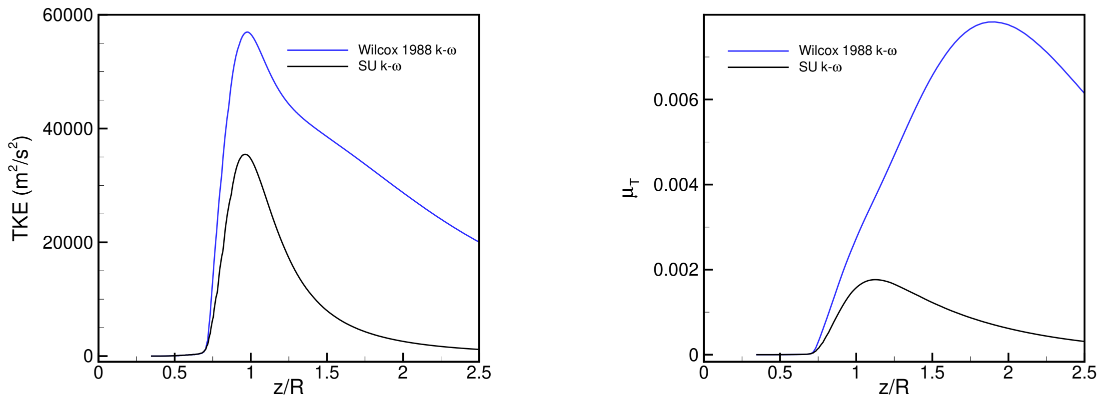

(a) **(b)**

Fig. 12 Variation of (a) turbulence kinetic energy TKE and (b) eddy viscosity μ_T along a streamline originating at the bottom nozzle lip, as shown in Fig. 11.

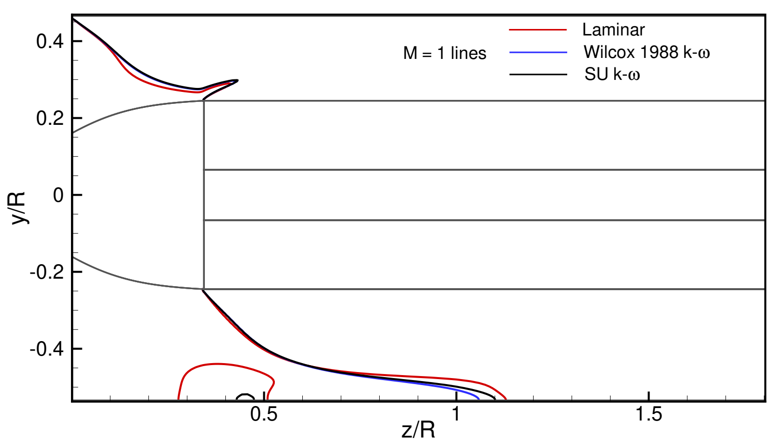

Fig. 13 Sonic lines depicting the expansion of jet boundaries as obtained using Laminar, Wilcox 1988 k-ω, and SU model computations.

VI. Conclusions

Multi-jet interaction involves a complex flowfield due to the various flow structures and inviscid/viscous interactions, flow regimes (from subsonic to supersonic) and large thermal and momentum gradients present within the base region. The interaction of adjacent under expanded jets can result in reverse flow of the jet exhaust gases towards the rocket base, and potentially cause high pressure and heat loads on the vehicle. The complex multi-nozzle configuration requires an elaborate grid generation and thus CFD simulation of these flows is an exceptionally challenging and computationally intensive task. In this work, we study the multi-jet interaction flowfield for the Musial and Ward [7] four-nozzle rocket system configuration using three-dimensional RANS computations. The simulations capture the flowfield features such as flow expansion around the base shoulder, free shear layer at the jet boundary and its interaction with the external supersonic flow, and the resulting shock waves.

The presence of shock waves interacting with the turbulent boundary layers and turbulent free shear layers makes the choice of shock-unsteadiness (SU) turbulence model more suitable for simulating such flows. We apply the SU k-ω model to this problem and perform a comparative study with the results obtained using laminar and Wilcox 1988 k-ω model computations. The shock-unsteadiness correction results in a lower amplification of turbulent kinetic energy at the shockwaves, and thus a reduced eddy viscosity in the shear layers. The location and strength of the shockwaves, and the reverse flow are not altered much. As a result, the base pressure predictions by the SU k-ω model are identical to that of the Wilcox 1988 k-ω, for the current case of a moderately expanded nozzle. At higher altitudes, with a higher nozzle pressure ratio, the shockwaves can be located closer to the vehicle, and a more significant effect of the shock-unsteadiness correction can be expected.

References

[1] Goethert, B.H., "Base flow characteristics of missiles with cluster-rocket exhausts," *Aerospace Engineering*, Vol. 20, No. 3, 1961, pp.28.

[2] Page, R.H., and Dixon, R.J., "Base Heating on a Multiple Propulsion Nozzle Missile," *AIAA paper*, Vol. 63, No. 179, 1963.

[3] Lamb, J.P., Abbud, K.A., and Lenzo, C.S., "A theory for base pressures on multinozzle rocket configurations," *Journal of Spacecraft and Rockets*, 7(4), 1970, pp.451-457.

[4] Marion, E.D., Daniels, D.J., Herstine, G.L., and Burge, G.W., "Exhaust Reversal from Cluster Nozzles - A New Flow Model", *ARS Paper* No. 62-2706, 1962.

[5] Taylor, R.A. and Tou, P.P., "Convective Heat Transfer in the Base Region of Large Space Boosters with Clustered Engines," *Procedure Heat Transfer Fluid Mechanics Institute*, Stanford University Press, 1967.

[6] Goethert, B.H. and Barnes, L.T., "Some studies of the flow pattern at the base of missiles with rocket exhaust jets," *AEDC-TR-58-12*, ARO Inc. Arnold AFS TN, 1960.

[7] Musial, N.T. and Ward, J.J., "Base flow characteristics for several four-clustered rocket configurations at mach numbers from 2.0 to 3.5," *NASA TN D-1093*, National Aeronautics and Space Administration, Washington DC, 1961.

[8] Charczenko, N. and Hayes, C., "Jet effects at supersonic speeds on base and afterbody pressures of a missile model having single and multiple jets," *NASA TN D-2046*, National Aeronautics and Space Administration, Washington DC, 1963.

[9] Cubbage, J.M., "Investigation of Exhaust Backflow from a Simulated Cluster of Three Wide-spaced Rocket Nozzles in a Near-space Environment," *NASA TN D-3016*, National Aeronautics and Space Administration, Hampton VA Langley Research Center, 1965.

[10] Wasko, R.A. and Cover, T.L., "Experimental investigation of base flow field at high altitudes for configurations of four and five clustered nozzles," *NASA TM X-1371*, National Aeronautics and Space Administration, Lewis Research Center, Cleveland, Ohio, 1967.

[11] Brewer, E.B. and Craven, C.E., "Experimental investigation of base flow field at high altitude for a four engine clustered nozzle configuration," *NASA TN D-5164*, National Aeronautics and Space Administration, Washington DC, 1969.

[12] Desikan, S.L.N., Murugan, B., Srinivasan, K. and Sajan, S., "Twin Jet Interaction and Reverse Flow," *Journal of Spacecraft and Rockets*, Vol.52, No.6, 2015, pp.1577-1585.

[13] Mehta, M., Dufrene, A.T., Seaford, M. and Knox, K., "Space Launch System Base Heating Test: Environments and Base Flow Physics," 54^{th} *AIAA Aerospace Sciences Meeting*, 2016, pp.0547.

[14] Mehta, M., Canabal, F., Tashakkor, S.B. and Smith, S.D., "Numerical Base Heating Sensitivity Study for a Four-Rocket Engine Core Configuration," *Journal of Spacecraft and Rockets*, Vol.50, No.3, 2013, pp.509-526.

[15] Nallasamy, R., Kandula, M., Duncil, L. and Schallhorn, P., "Numerical Simulation of the Base Flow and Heat Transfer Characteristics of a Four-Nozzle Clustered Rocket Engine," 40^{th} *Thermophysics Conference*, 2008, pp.4128.

[16] Ebrahimi, H., "Numerical investigation of multi-plume rocket rhenomenology," 33^{rd} *Joint Propulsion Conference and Exhibit*, July 1997, pp.2942.

[17] Wang, T.S., "Numerical analysis of base flowfield for a four-engine clustered nozzle configuration," *Journal of Propulsion and Power*, Vol.11, No.5, 1995, pp.1076-1078.

[18] Gusman, M., Housman, J. and Kiris, C., "Best Practices for CFD simulations of launch vehicle ascent with plumes-overflow perspective," 49^{th} *AIAA Aerospace Sciences Meeting including the New Horizons Forum and Aerospace Exposition*, 2011, pp.1054.

[19] Deere, K., Elmiligui, A. and Abdol-Hamid, K.S., "USM3D Simulations of Saturn V Plume-Induced Flow Separation," *Journal of Spacecraft and Rockets*, Vol.49, No.4, 2012, pp.679-690.

[20] Sinha, K., Mahesh K., and Candler G. V., "Modeling shock unsteadiness in shock/turbulence interaction," *Physics of Fluids*, Vol.15, No.8, 2003, pp. 2290-2297.

[21] Sinha, K., Mahesh, K. and Candler, G.V., "Modeling the effect of shock unsteadiness in shock/turbulent boundary-layer interactions," *AIAA Journal*, Vol.43, No.3, 2005, pp.586-594.

[22] Pasha, A. A., and Sinha K., "Shock-unsteadiness model applied to oblique shock wave/turbulent boundary-layer interaction," *International Journal of Computational Fluid Dynamics*, Vol.22, No.8, 2008, pp. 569-582.

[23] Pasha, A. A., and Sinha K., "Simulation of hypersonic shock/turbulent boundary-layer interactions using shock-unsteadiness model," *Journal of Propulsion and Power*, Vol.28, No.1, 2012, pp.46-60.

[24] Roy, S., Pathak, U. and Sinha, K., "Variable turbulent Prandtl number model for shock/boundary-layer interaction," *AIAA J.*, Vol.56, No.1, 2017, pp.342-355.

[25] Emami, B., Bussmann, M. and Tran, H., "Application of realizability and shock unsteadiness to k-ϵ simulations of under-expanded axisymmetric supersonic free jets," *Journal of Fluids Engineering*, Vol.132, No.4, 2010, pp.041104.

[26] Wilcox, D. C., "Turbulence Modeling for CFD," DCW, La Canada, CA. 3rd edition, 2006.

[27] Candler, G.V., Sinha, K., and Levin, D.A., "Numerical simulations of Atlas-II rocket motor plumes," 39^{th} *AIAA Aerospace Sciences Meeting and Exhibit Reno*, 2001.

[28] Reddy, D.S.K., Sinha, K., "Hypersonic turbulent flow simulation of Fire II reentry vehicle afterbody," *Journal of Spacecraft and Rockets*, Vol.46, No.4, 2009, pp.745-757.

[29] Reddy, D.S.K., Sinha, K., "Effect of Chemical Reaction Rates on Aeroheating Predictions of Reentry Flows," *Journal of Thermophysics and Heat Transfer*, Vol.25, No.1, 2011, pp.21-33.

[30] Reddy, D.S.K., Saikia, B., Sinha, K., "Effect of High-Enthalpy Air Chemistry on Stagnation Point Heat Flux," *Journal Of Thermophysics And Heat Transfer*, Vol.28, No.2, 2014, pp.356-359.

[31] MacCormack, R.W., Candler, G.V., "The solution of the Navier-Stokes equations using Gauss-Seidel line relaxation," *Computers & fluids*, Vol.17, No.1, 1989, pp.135-150.

[32] Wright, M. J., Candler, G. V., and Bose, D., "Data-Parallel Line Relaxation Method for the Navier-Stokes Equations," *AIAA Journal*, Vol.36, No.9, 1998, pp.1603-1609.